

KA-TP-23-2001

November 8, 2018

hep-ph/0109103

$O(\alpha_s)$ Corrections to $b\bar{b} \rightarrow W^\pm H^\mp$ at the CERN Large Hadron Collider

WOLFGANG HOLLIK AND SHOU-HUA ZHU

*Institut für Theoretische Physik, Universität Karlsruhe,
D-76128 Karlsruhe, Germany*

The $O(\alpha_s)$ corrections to the cross section for $b\bar{b} \rightarrow W^\pm H^\mp$ at the LHC are calculated in the minimal supersymmetric standard model (MSSM) in the \overline{MS} and OS (on-mass-shell) renormalization schemes. The results in two schemes are in good agreement. In the \overline{MS} scheme, the QCD corrections are negative and within $-14\% \sim -20\%$ for charged Higgs mass up to 1 TeV and $\tan\beta > 15$. For $\tan\beta = 2$, the magnitude of the QCD corrections can be greater than 30%.

PACS number: 12.60.Jv, 12.15.Lk, 14.80.Cp, 14.70.Fm

I. INTRODUCTION

The detection of Higgs particles is one of the most important objectives of the Large Hadron Collider (LHC). Charged Higgs bosons are predicted in extended versions of the Standard model (SM), like two-Higgs-doublet models (2HDM) and the Minimal Supersymmetric Standard Model (MSSM). A discovery of such an additional Higgs boson will immediately indicate physics beyond the SM; there is, hence, strong theoretical and experimental activity to provide the basis for its accurate exploration.

At hadron colliders, the charged Higgs boson H^\pm could appear as the decay product of primarily produced top quarks if the mass of H^\pm is smaller than $m_t - m_b$. For heavier H^\pm , other mechanism for H^\pm production have been investigated: single Higgs-boson production associated with heavy quarks, like $gb \rightarrow H^- t$ [1] and $qb \rightarrow q' b H^-$ [2], and pair production of H^\pm through tree-level $q\bar{q}$ annihilation and via the loop-induced gluon-fusion mechanism [3]. Moreover, single H^\pm production in association with a W boson, via tree-level $b\bar{b}$ annihilation and one-loop gg fusion has been proposed and analyzed [4]. Detailed studies [5] show that these production mechanisms at the LHC can help to explore the parameter space, even beyond $m_{H^\pm} \sim 1\text{TeV}$ and down to at least $\tan\beta \sim 3$.

Since $b\bar{b}$ annihilation is the main source of the hadronic $W^\pm H^\mp$ production cross section, it is necessary to calculate and implement also the loop contributions to $b\bar{b} \rightarrow W^\pm H^\mp$ for more accurate theoretical predictions. Recently, the calculation of the $O(\alpha_{ew} m_{t(b)}^2/m_W^2)$ and $O(\alpha_{ew} m_{t(b)}^4/m_W^4)$ supersymmetric electroweak(EW) one-loop corrections were presented in [6] in the frame of the MSSM, which can give rise to a 10-15% reduction of the lowest-order result. In this paper, we deal with the one-loop QCD corrections to $b\bar{b} \rightarrow W^\pm H^\mp$.

The arrangement of this paper is as follows. Section II contains the analytic results, and in Section III we present numerical examples and discuss the implications of our results. The lengthy expressions of the form factors are collected in the Appendix.

II. ANALYTIC EXPRESSIONS

A. Virtual corrections

The Feynman diagrams for charged Higgs-boson production via the parton process $b(p_1)\bar{b}(p_2) \rightarrow H^-(k_1)W^+(k_2)$, including the QCD corrections, are shown in Fig. 1. The diagrams are created by use of FeynArts [7] and are handled with the help of FeynCalc [8]. We keep the finite b -quark mass throughout the calculation, in order to control the collinear divergences.

As usual, we define the Mandelstam variables as

$$\begin{aligned}\hat{s} &= (p_1 + p_2)^2 = (k_1 + k_2)^2, \\ \hat{t} &= (p_1 - k_1)^2 = (p_2 - k_2)^2, \\ \hat{u} &= (p_1 - k_2)^2 = (p_2 - k_1)^2.\end{aligned}\tag{1}$$

Taking into account the $O(\alpha_s)$ corrections, the renormalized amplitude for $b\bar{b} \rightarrow W^+H^-$ can be written in the following way,

$$\begin{aligned}M_{\text{ren}} &= M_0^{(s)} + M_0^{(t)} + \delta\hat{M}^{V_1(s)}(H) + \delta\hat{M}^{V_1(s)}(h) + \delta\hat{M}^{V_1(s)}(A) \\ &\quad + \delta\hat{M}^{V_1(t)} + \delta\hat{M}^{S(t)} + \delta\hat{M}^{V_2(t)} + \delta M^{\text{box}}.\end{aligned}\tag{2}$$

$M_0^{(s)}$ and $M_0^{(t)}$ are the s - and t -channel tree-level diagrams corresponding to Fig. 1(a) and Fig. 1(b), which are given by

$$\begin{aligned}M_0^{(s)} &= \frac{gh_b}{\sqrt{2}} \left[-\frac{\cos\alpha \sin(\alpha - \beta)}{\hat{s} - m_H^2} + \frac{\sin\alpha \cos(\alpha - \beta)}{\hat{s} - m_h^2} \right] (M_5 + M_6 + M_9 + M_{10}) \\ &\quad + \frac{gh_b \sin\beta}{\sqrt{2}(\hat{s} - m_A^2)} (M_5 - M_6 + M_9 - M_{10}), \\ M_0^{(t)} &= \frac{g}{\sqrt{2}(\hat{t} - m_t^2)} [h_b \sin\beta (2M_9 + m_b M_1 + M_3) - h_t m_t \cos\beta M_2],\end{aligned}\tag{3}$$

where

$$h_b = \frac{gm_b}{\sqrt{2}m_W \cos\beta}, \quad h_t = \frac{gm_t}{\sqrt{2}m_W \sin\beta}\tag{4}$$

denote the Yukawa couplings of the bottom and top quarks. M_i are reduced standard matrix elements, which are defined by

$$\begin{aligned}
M_1 &= \bar{v}(p_2) \not{\epsilon}(k_2) P_R u(p_1), \\
M_2 &= \bar{v}(p_2) \not{\epsilon}(k_2) P_L u(p_1), \\
M_3 &= \bar{v}(p_2) \not{k}_2 \not{\epsilon}(k_2) P_R u(p_1), \\
M_4 &= \bar{v}(p_2) \not{k}_2 \not{\epsilon}(k_2) P_L u(p_1), \\
M_5 &= \bar{v}(p_2) P_R u(p_1) p_1 \cdot \epsilon(k_2), \\
M_6 &= \bar{v}(p_2) P_L u(p_1) p_1 \cdot \epsilon(k_2), \\
M_7 &= \bar{v}(p_2) \not{k}_2 P_R u(p_1) p_1 \cdot \epsilon(k_2), \\
M_8 &= \bar{v}(p_2) \not{k}_2 P_L u(p_1) p_1 \cdot \epsilon(k_2), \\
M_9 &= \bar{v}(p_2) P_R u(p_1) p_2 \cdot \epsilon(k_2), \\
M_{10} &= \bar{v}(p_2) P_L u(p_1) p_2 \cdot \epsilon(k_2), \\
M_{11} &= \bar{v}(p_2) \not{k}_2 P_R u(p_1) p_2 \cdot \epsilon(k_2), \\
M_{12} &= \bar{v}(p_2) \not{k}_2 P_L u(p_1) p_2 \cdot \epsilon(k_2),
\end{aligned} \tag{5}$$

with the projectors $P_{L,R} \equiv (1 \mp \gamma_5)/2$.

The terms $\delta\hat{M}$ in (2) describe the virtual contributions from the 2- and 3-point functions together with their counterterms, and δM^{box} denotes the contribution from the irreducible 4-point function. The vertex and self-energy corrections to the tree-level process are included in $\delta\hat{M}^{V,S}$, which are given by

$$\begin{aligned}
\delta\hat{M}^{V_1(s)}(H, h) &= \frac{gh_b}{\sqrt{2}} \left[-\frac{\cos\alpha \sin(\alpha - \beta)}{\hat{s} - m_H^2}, \frac{\sin\alpha \cos(\alpha - \beta)}{\hat{s} - m_h^2} \right] (M_5 + M_6 + M_9 + M_{10}) \\
&\quad \times \left[\frac{\delta m_b}{m_b} + \frac{1}{2} \delta Z_L^b + \frac{1}{2} \delta Z_R^b \right] + \delta M^{V_1(s)}(H, h), \\
\delta\hat{M}^{V_1(s)}(A) &= \frac{gh_b \sin\beta}{\sqrt{2}(\hat{s} - m_A^2)} \left[\frac{\delta m_b}{m_b} + \frac{1}{2} \delta Z_L^b + \frac{1}{2} \delta Z_R^b \right] (M_5 - M_6 + M_9 - M_{10}) + \delta M^{V_1(s)}(A), \\
\delta\hat{M}^{V_1(t)} &= \frac{g}{\sqrt{2}(\hat{t} - m_t^2)} [h_b \sin\beta (2M_9 + m_b M_1 + M_3) - h_t m_t \cos\beta M_2] \\
&\quad \times \left(\frac{1}{2} \delta Z_L^t + \frac{1}{2} \delta Z_L^b \right) + \delta M^{V_1(t)}, \\
\delta\hat{M}^{S(t)} &= \frac{g}{\sqrt{2}(\hat{t} - m_t^2)^2} [h_b \sin\beta (2M_9 + m_b M_1 + M_3) (2m_t \delta m_t + (m_t^2 - \hat{t}) Z_L^t) \\
&\quad - h_t \cos\beta M_2 (\delta m_t (m_t^2 + \hat{t}) + m_t (m_t^2 - \hat{t}) Z_L^t)] + \delta M^{S(t)}, \\
\delta\hat{M}^{V_2(t)} &= \frac{g}{\sqrt{2}(\hat{t} - m_t^2)} [h_b \sin\beta (2M_9 + m_b M_1 + M_3) \left(\frac{\delta m_b}{m_b} + \frac{1}{2} Z_R^t + \frac{1}{2} Z_L^b \right)
\end{aligned}$$

$$-h_t m_t \cos \beta M_2 \left(\frac{\delta m_t}{m_t} + \frac{1}{2} Z_L^t + \frac{1}{2} Z_R^b \right) + \delta M^{V_2(t)}. \quad (6)$$

Therein, $\delta M^{V_1(s)}(H, h, A)$, $\delta M^{V_1(t)}$, $\delta M^{S(t)}$, $\delta M^{V_2(t)}$ represent the unrenormalized one-loop corrections arising, respectively, from the $b\bar{b}H(h, A)$ vertex diagrams in Fig. 1(c), the $\bar{t}bH^-$ vertex diagram Fig. 1(d), the $\bar{b}tW^+$ vertex diagram Fig. 1(e), and the top-quark self-energy diagram Fig. 1(f); δM^{box} corresponds to the box diagram Fig. 1(g). All the $\delta M^{V,S}$ and δM^{box} can be written in the form

$$\delta M = C_F \sum_{i=1}^{12} f_i M_i, \quad C_F = \frac{4}{3}, \quad (7)$$

with the reduced matrix elements M_i in (5) and form factors f_i , which are given explicitly in the Appendix.

Here we present the analytical results in the \overline{MS} scheme; accordingly, the quark masses in (4) are running masses $m_{b,t}(\mu)$. The results in the OS scheme can be easily obtained by using the pole masses and replacing the corresponding field- and mass-renormalization constants. Actually in the \overline{MS} scheme, we must add the finite part of the wave-function renormalization constants for the b quarks, according to the LSZ prescription.

From the self-energy diagram in Fig. 1(h) for the b, t quarks we get the explicit expressions of the renormalization constants, valid for both the t and b quark,

$$\begin{aligned} \frac{\delta m}{m} &= -\frac{\alpha_s}{4\pi} 3C_F \Delta, \\ Z_L &= Z_R = -\frac{\alpha_s}{4\pi} C_F \Delta, \quad \text{with} \\ \Delta &= \frac{2}{\epsilon} - \gamma_E + \log(4\pi), \quad \epsilon = 4 - D, \end{aligned} \quad (8)$$

in dimensional regularization.

Squaring the amplitude and performing the spin summations,

$$\overline{\sum} |M_{\text{ren}}|^2 = \overline{\sum} |M_0^{(s)} + M_0^{(t)}|^2 + 2 \text{Re} \overline{\sum} \delta M (M_0^{(s)} + M_0^{(t)})^\dagger, \quad (9)$$

yield the partonic cross section for the process $b\bar{b} \rightarrow W^+ H^-$ with virtual corrections,

$$\hat{\sigma}_{b\bar{b} \rightarrow W^+ H^-}^{\text{virt}}(\hat{s}) = \int_{t_-}^{\hat{t}_+} d\hat{t} \frac{1}{16\pi \hat{s}^2} \overline{\sum} |M_{\text{ren}}|^2 \quad (10)$$

with

$$\hat{t}_{\pm} = \frac{m_W^2 + m_{H^\pm}^2 - \hat{s}}{2} \pm \frac{1}{2} \sqrt{(\hat{s} - (m_W + m_{H^\pm})^2)(\hat{s} - (m_W - m_{H^\pm})^2)}. \quad (11)$$

The partonic cross section $\hat{\sigma}_{b\bar{b} \rightarrow W^- H^+}^{\text{virt}}$ for the process $b\bar{b} \rightarrow W^- H^+$ is identical to that of $b\bar{b} \rightarrow W^+ H^-$.

B. Real-gluon contributions

The virtual corrections involve an infrared singularity from the massless gluon. For our purpose, we can use a small gluon mass λ for regularization, which allows to identify the infrared divergence as a $\log(\lambda)$ term. This infrared divergence is cancelled by adding the corresponding real-gluon-radiation corrections, displayed in Fig. 1(i-m). For technical reasons, it is convenient to perform the phase-space integration over a soft- and hard-gluon part separately. The soft-gluon contribution to the cross section at the partonic level is proportional to the tree-level cross section $\hat{\sigma}_{b\bar{b} \rightarrow H^\pm W^\mp}^0$ for $b\bar{b} \rightarrow H^\pm W^\mp$,

$$\begin{aligned} \hat{\sigma}^{\text{soft}} &= \hat{\sigma}_{b\bar{b} \rightarrow H^\pm W^\mp}^0 \delta_s, \\ \delta_s &= -C_F \frac{\alpha_s}{2\pi} \left\{ \log \frac{4\Delta E^2}{\lambda^2} + \log \frac{m_b^2}{\hat{s}} + \log \frac{m_b^2}{\hat{s}} \log \frac{4\Delta E^2}{\lambda^2} + \frac{\pi^2}{3} + \frac{1}{2} \log^2 \left(\frac{m_b^2}{\hat{s}} \right) \right\}, \end{aligned} \quad (12)$$

where ΔE is the energy cutoff for soft gluons. After adding the cross section (10) with the virtual corrections, the sum is independent on λ , and the \log^2 term cancels.

For the hard-gluon part, we use the Monte Carlo packages BASES [9] to perform the phase space integration, with the cutoff that the energy of the gluon is greater than ΔE . We do not give detailed expressions here. Numerically it was checked that the sum $\hat{\sigma}^{\text{soft}} + \hat{\sigma}^{\text{hard}}$ is independent of the cutoff ΔE .

At $O(\alpha_s)$, there are also initial-gluon contributions from $gb \rightarrow bW^\pm H^\mp$, the Feynman diagrams can be obtained from Fig. 1(i-m) by treating gluon and b quark as incoming partons. For the processes, we should caution how to subtract the on-shell top quark and/or charged Higgs boson contributions. Following the methods of Ref. [10], the partonic cross section after subtracting the on-shell contributions of subprocess $gb \rightarrow bW^\pm H^\mp$ can be written as:

$$\begin{aligned} \hat{\sigma}_{gb \rightarrow bW^\pm H^\mp}^{0, \text{sub}} &= \hat{\sigma}_{gb \rightarrow bW^\pm H^\mp}^0 - \hat{\sigma}_{gb \rightarrow tH^\mp}^0 Br(t \rightarrow bW^+) \\ &\quad - \hat{\sigma}_{gb \rightarrow tW^-}^0 Br(t \rightarrow bH^+). \end{aligned} \quad (13)$$

The cross section of $g\bar{b} \rightarrow \bar{b}W^\pm H^\mp$ can be obtained similarly.

C. Hadronic cross section and subtracting double counting

In the approach described above we have considered the real-gluon corrections, which give rise to a term involving $\log(\hat{s}/m_b^2)$ from the region where the b quark splits into a collinear b -quark–gluon pair and the gluon into a collinear b pair. This logarithm is already contained in the heavy-quark distribution function, hence it has to be removed. This can be done, following [11], by subtracting the tree-level process $b\bar{b} \rightarrow H^\pm W^\mp$ convoluted with one heavy-quark distribution function given by the perturbative solution to DGLAP equation,

$$\begin{aligned}\tilde{b}_{(bb)}(x, \mu_f) &= \frac{\alpha_s(\mu)}{2\pi} \log\left(\frac{\mu_f^2}{m_b^2}\right) \int_x^1 \frac{dy}{y} P_{qq}\left(\frac{x}{y}\right) b(y, \mu_f), \\ \tilde{b}_{(bg)}(x, \mu_f) &= \frac{\alpha_s(\mu)}{2\pi} \log\left(\frac{\mu_f^2}{m_b^2}\right) \int_x^1 \frac{dy}{y} P_{qg}\left(\frac{x}{y}\right) g(y, \mu_f),\end{aligned}\tag{14}$$

where

$$\begin{aligned}P_{qq}(z) &= C_F \left[\frac{1+z^2}{(1-z)_+} + \frac{3}{2} \delta(1-z) \right], \\ P_{qg}(z) &= \frac{1}{2} [z^2 + (1-z)^2].\end{aligned}\tag{15}$$

In this way, the total cross section at $O(\alpha_s)$ can be expressed as

$$\begin{aligned}\sigma^{NLO} &= \bar{b} \otimes \hat{\sigma}_{b\bar{b}} \otimes b - \tilde{b}_{(bb)} \otimes \hat{\sigma}_{b\bar{b} \rightarrow H^\pm W^\mp}^0 \otimes b - \bar{b} \otimes \hat{\sigma}_{b\bar{b} \rightarrow H^\pm W^\mp}^0 \otimes \tilde{b}_{(bb)} \\ &\quad + b \otimes \hat{\sigma}_{bg \rightarrow bH^\pm W^\mp}^{0,sub} \otimes g - b \otimes \hat{\sigma}_{b\bar{b} \rightarrow H^\pm W^\mp}^0 \otimes \tilde{b}_{(bg)} \\ &\quad + \bar{b} \otimes \hat{\sigma}_{\bar{b}g \rightarrow \bar{b}H^\pm W^\mp}^{0,sub} \otimes g - \bar{b} \otimes \hat{\sigma}_{b\bar{b} \rightarrow H^\pm W^\mp}^0 \otimes \tilde{b}_{(bg)},\end{aligned}\tag{16}$$

where $\hat{\sigma}_{b\bar{b}}$ is the infrared-finite parton cross section which is given by the sum of $\hat{\sigma}^{\text{virt}} + \hat{\sigma}^{\text{soft}} + \hat{\sigma}^{\text{hard}}$. In eq. (16), $A \otimes \hat{\sigma} \otimes B$ represents the cross section of the subprocess $\hat{\sigma}$ is convoluted with the parton distribution functions (PDF) A and B ,

$$A \otimes \hat{\sigma} \otimes B = \int_{z_0}^1 dz \frac{dL}{dz} \hat{\sigma}(z^2 s), \quad z_0 = \frac{m_W + m_{H^\pm}}{\sqrt{s}},\tag{17}$$

where \sqrt{s} is the overall CM energy of the pp system, and the parton luminosity dL/dz is defined as

$$\frac{dL}{dz} = 2z \int_{z^2}^1 \frac{dx}{x} A(x, \mu_f) B\left(\frac{z^2}{x}, \mu_f\right).\tag{18}$$

III. NUMERICAL RESULTS

We now present a numerical discussion of the QCD corrections to $W^\pm H^\mp$ associated production at the LHC. The SM input parameters in our calculations were taken to be $\alpha_{ew}(m_Z) = 1/128.8$, $\alpha_s(m_Z) = 0.118$, $m_W = 80.41\text{GeV}$ and $m_Z = 91.1867\text{GeV}$, and the pole masses of top and bottom quarks are $m_t = 175\text{GeV}$ and $m_b = 4.7\text{GeV}$. We have used the two-loop running \overline{MS} quark masses [12] and strong coupling constant [13], the CTEQ5M PDF [14], and we choose the factorization and renormalization scale as $m_{H^\pm} + m_W$, if not stated otherwise. The expressions given in the previous section are valid for a general Two-Higgs-doublet model; they cover the MSSM case for a specific choice of the Higgs-boson masses and mixing angles. Here we focus on the MSSM scenario, taking into account the one-loop relations [15] between the Higgs-boson masses M_{h,H,A,H^\mp} and the angles α and β , with m_{H^\pm} and β chosen as the two independent Higgs-input parameters, together with $M_S = 1\text{ TeV}$ as a genuine SUSY mass scale. As a remark, the SUSY-QCD corrections arising from virtual gluino and squarks may also become important for specific parameters, which will be studied separately.

In Fig. 2 we present the total cross sections, for the $b\bar{b}$ -annihilation subprocess, in the \overline{MS} and OS renormalization schemes, and the relative deviation $\Delta = (\sigma^{OS} - \sigma^{\overline{MS}})/(\sigma^{OS} + \sigma^{\overline{MS}})$ in Fig. 3, both as functions of m_{H^\pm} . The results differ remarkably at tree-level (LO) and are significantly closer at the level including the QCD corrections (NLO). Whereas in the OS scheme the LO cross section is sizeably reduced at NLO, the cross section increases in the \overline{MS} scheme at NLO.

For $\tan\beta = 50$, Δ is still relatively large, around 8%, which can, however, be easily understood as a higher-order effect. For large $\tan\beta$ we can write the cross section in the two schemes as

$$\begin{aligned}\sigma^{OS} &\propto m_{b,pole}^2 (1 - A + B), \\ \sigma^{\overline{MS}} &\propto m_b(\mu)^2 (1 + B),\end{aligned}\tag{19}$$

with

$$A = 2\frac{\alpha_s}{\pi}(\log\frac{\mu^2}{m_b^2} + \frac{4}{3}),\tag{20}$$

which is the quantity entering also the relation between the \overline{MS} quark mass and the corresponding pole mass at one-loop order,

$$m(\mu)^2 = m_{pole}^2 \left[1 - 2 \frac{\alpha_s}{\pi} \left(\log \frac{\mu^2}{m^2} + \frac{4}{3} \right) \right]. \quad (21)$$

Hence, one finds

$$\Delta \simeq AB/2. \quad (22)$$

For $\mu = 200 \text{ GeV}$, we have $A \simeq 0.6$, $B \simeq 0.3$ and $\Delta \simeq 9\%$. In the following we will give the results only in the \overline{MS} scheme, which is usually more stable with respect to missing higher-order terms.

Fig. 4 and Fig. 5 show the LO tree-level cross section σ^0 and the NLO cross section σ^{NLO} , including the bg contribution, as well as the relative correction $\delta = (\sigma^{NLO} - \sigma^0)/\sigma^0$ as a function of m_{H^\pm} and $\tan\beta$. As pointed out before, due to the competition between the top-Higgs and bottom-Higgs Yukawa couplings, the cross sections are relatively small for intermediate values of $\tan\beta$, around $\tan\beta \sim 6$ (see Fig. 6). From the figures, we can see that the QCD corrections are negative and the magnitude is greater than 14% for all charged Higgs mass and $\tan\beta$. For $\tan\beta = 2$, the QCD corrections can decrease the cross section more than 30%. Table 1 contains numerical results for the relative correction δ for a low and a high value of $\tan\beta$, $\tan\beta = 2$ and 50.

Fig. 6 and 7 display the LO and NLO hadronic cross section and the relative correction δ as a function of $\tan\beta$, for $m_{H^\pm} = 200, 500$ and 1000 GeV . From the figures, one can see that the QCD corrections are almost independent of $\tan\beta$ when $\tan\beta > 15$. For $\tan\beta < 15$, the magnitude of the QCD corrections decreases with the increment of $\tan\beta$.

In Fig. 8 we present the uncertainty of varying the factorization scale, which is defined as

$$\frac{\sigma(\mu_f = 2\mu_0) - \sigma(\mu_f = \frac{1}{2}\mu_0)}{\sigma(\mu_f = \mu_0)} \quad (23)$$

with $\mu_0 = m_{H^\pm} + m_W$, as a function of m_{H^\pm} . We can see that the uncertainty is less than 10% for all the charged Higgs boson mass and $\tan\beta$.

IV. CONCLUSION

In conclusion, we have calculated the $O(\alpha_s)$ corrections to the cross sections for $b\bar{b} \rightarrow W^\pm H^\mp$ associated production at the LHC in both \overline{MS} and OS renormalization schemes, with an explicit discussion for the charged Higgs boson of the MSSM. The results in these two schemes are in good agreement. Our numerical NLO results include also the contributions from $gb \rightarrow bH^\pm W^\mp$. In the \overline{MS} scheme, the QCD corrections are negative and within $-14\% \sim -20\%$ for charged Higgs mass up to 1 TeV and $\tan\beta > 15$. For $\tan\beta = 2$, the magnitude of the QCD corrections can be greater than 30%.

The analytical results given in this paper are also valid in a general 2-Higgs-doublet model, where the constraints among Higgs masses and angles α and β are released. As a final remark, the higher-order contributions arising from the $gg \rightarrow H^\pm W^\mp b\bar{b}$, may also be important, especially for lower values of the charged Higgs-boson mass. They are presently under investigation.

V. ACKNOWLEDGEMENT

S.H. Zhu would like to thank Prof. C.S. Li for the stimulating discussion in the first stage of this work, and Prof. W.-K. Tung for the suggestion on PDF. This work was supported in part by the Alexander von Humboldt Foundation, National Nature Science Foundation of China and the Deutsche Forschungsgemeinschaft. Parts of the calculations have been performed on the QCM cluster at the University of Karlsruhe, supported by the DFG-Forschergruppe "Quantenfeldtheorie, Computeralgebra und Monte-Carlo-Simulation".

VI. APPENDIX

In this Appendix, we will present the non-vanishing form factors in the decomposition (7) of the various s - and t -channel contributions to the one-loop matrix element. The form factors contributing to $\delta M^{S(t)}$ are

$$\begin{aligned}
f_1 &= -\frac{\alpha_s g h_b m_b \sin \beta}{4\sqrt{2}\pi(m_t^2 - \hat{t})^2 \hat{t}} [(3m_t^2 - \hat{t})\hat{t} - m_t^2(m_t^2 + \hat{t})B_0(0, 0, m_t^2) \\
&\quad + (m_t^4 - 6m_t^2 \hat{t} + \hat{t}^2)B_0(\hat{t}, 0, m_t^2)], \\
f_2 &= -\frac{\alpha_s g h_t m_t \cos \beta}{2\sqrt{2}\pi(m_t^2 - \hat{t})^2} [-m_t^2 + m_t^2 B_0(0, 0, m_t^2) + (m_t^2 + \hat{t})B_0(\hat{t}, 0, m_t^2)], \\
f_3 &= f_1/m_b, \\
f_9 &= 2f_1/m_b.
\end{aligned} \tag{24}$$

The form factors that contribute to $\delta M^{V_1(t)}$ are (the argument the C functions is $[m_b^2, \hat{t}, m_w^2, m_b^2, \lambda^2, m_t^2]$)

$$\begin{aligned}
f_1 &= \frac{\alpha_s g h_b m_b \sin \beta}{4\sqrt{2}\pi(m_t^2 - \hat{t})} [1 - 2B_0(\hat{t}, \lambda^2, m_t^2) - 2(m_b^2 + m_t^2)C_0 - 2m_w^2(C_1 + C_2) + 4C_{00}], \\
f_2 &= \frac{\alpha_s g h_t m_t \cos \beta}{4\sqrt{2}\pi(m_t^2 - \hat{t})} [-1 + 2B_0(\hat{t}, \lambda^2, m_t^2) + 4m_b^2 C_0 + 2(m_b^2 + m_w^2 - \hat{t})C_1 + 2m_w^2 C_2 - 4C_{00}], \\
f_3 &= \frac{\alpha_s g h_b \sin \beta}{4\sqrt{2}\pi(m_t^2 - \hat{t})} [1 - 2B_0(\hat{t}, \lambda^2, m_t^2) - 2m_b^2 C_0 - 2(m_w^2 - \hat{t})C_1 - 2m_w^2 C_2 + 4C_{00}], \\
f_4 &= \frac{\alpha_s g h_t m_t m_b \cos \beta}{2\sqrt{2}\pi(m_t^2 - \hat{t})} [C_0 + C_1], \\
f_9 &= -\frac{\alpha_s g h_b \sin \beta}{2\sqrt{2}\pi(m_t^2 - \hat{t})} [-1 + 2B_0(\hat{t}, \lambda^2, m_t^2) + 2m_b^2 C_0 - 2(m_b^2 + m_t^2 - m_w^2)C_1 + 2m_w^2 C_2 \\
&\quad - 4C_{00} - 2m_b^2 C_{11} - 2(m_b^2 - \hat{t})C_{12}], \\
f_{10} &= \frac{\alpha_s g h_t m_t m_b \cos \beta}{\sqrt{2}\pi(m_t^2 - \hat{t})} [C_0 + 2C_1 + C_{11}], \\
f_{11} &= \frac{\alpha_s g h_b m_b \sin \beta}{\sqrt{2}\pi(m_t^2 - \hat{t})} [C_1 + C_{11} + C_{12}], \\
f_{12} &= -\frac{\alpha_s g h_t m_t \cos \beta C_{12}}{\sqrt{2}\pi(m_t^2 - \hat{t})}.
\end{aligned} \tag{25}$$

The form factors that contribute to δM^{box} are (the argument of the C and D functions is $[m_b^2, m_b^2, \hat{s}, m_b^2, \lambda^2, m_b^2]$ and $[m_{H^\pm}^2, m_b^2, m_b^2, m_w^2, \hat{t}, \hat{s}, m_t^2, m_b^2, \lambda^2, m_b^2]$)

$$f_1 = \frac{\alpha_s g m_b}{2\sqrt{2}\pi} [h_t m_b m_t \cos \beta (D_0 + D_2) + h_b \sin \beta (C_0 + m_t^2 D_0 + m_{H^\pm}^2 D_1$$

$$\begin{aligned}
& +(m_{H^\pm}^2 + m_w^2 - \hat{u})D_2 - (m_b^2 - \hat{u})D_3)], \\
f_2 = & \frac{\alpha_s g}{2\sqrt{2}\pi} [h_t m_t \cos \beta (-C_0 + (m_b^2 - m_t^2 - \hat{u})D_0 + (m_b^2 - m_{H^\pm}^2 - \hat{u})D_1 \\
& +(m_b^2 - m_{H^\pm}^2 - m_w^2)D_2 + (m_b^2 - m_w^2 - \hat{u})D_3 + 2D_{00}) \\
& + h_b m_b \sin \beta (-C_0 - m_t^2 D_0 + (m_b^2 - \hat{u})D_1 - \hat{t} D_2 \\
& - m_w^2 D_3 + 2D_{00})], \\
f_3 = & \frac{\alpha_s g}{2\sqrt{2}\pi} [h_t m_b m_t \cos \beta (D_0 + D_1 + D_2 + D_3) + h_b \sin \beta (m_b^2 (D_1 + D_3) - (2m_b^2 - \hat{s})D_2)], \\
f_4 = & -\frac{\alpha_s g m_b}{2\sqrt{2}\pi} [h_t m_t \cos \beta (D_0 + D_1 + D_2 + D_3) + h_b m_b \sin \beta (D_1 + D_3)], \\
f_5 = & \frac{\alpha_s g}{\sqrt{2}\pi} [h_t m_b m_t \cos \beta D_{11} + h_b \sin \beta (2C_0 + m_t^2 D_0 + (C_1 + C_2) \\
& - m_t^2 D_1 + \hat{t} D_2 + m_w^2 D_3 - 2D_{00} + (m_b^2 - 2m_{H^\pm}^2)D_{11} \\
& +(m_b^2 - m_{H^\pm}^2 - \hat{t})D_{12} + (2m_b^2 - \hat{t} - \hat{u})D_{13})], \\
f_6 = & -\frac{\alpha_s g m_b}{\sqrt{2}\pi} [h_t m_t \cos \beta (D_0 + 2D_1 + D_2 + D_{11} + D_{12}) + h_b m_b \sin \beta (D_1 + D_{11} + D_{12})], \\
f_7 = & \frac{\alpha_s g h_b m_b D_3 \sin \beta}{\sqrt{2}\pi}, \\
f_8 = & -\frac{\alpha_s g}{\sqrt{2}\pi} [h_t m_t \cos \beta (D_0 + 2D_1 + D_2 + D_3 + D_{11} + D_{12} + D_{13}) \\
& + h_b m_b \sin \beta (D_1 + D_{11} + D_{12} + D_{13})], \\
f_9 = & \frac{\alpha_s g}{\sqrt{2}\pi} [h_t m_b m_t \cos \beta (D_{11} + D_{12}) + h_b \sin \beta (2C_0 + m_t^2 (D_0 - D_1) \\
& + C_2 + (m_b^2 - m_t^2 + m_w^2 - \hat{u})D_2 + m_w^2 D_3 - 2D_{00} \\
& +(m_b^2 - 2m_{H^\pm}^2)D_{11} + (2m_b^2 - 3m_{H^\pm}^2 - \hat{t})D_{12} \\
& +(2m_b^2 - \hat{t} - \hat{u})D_{13} + (m_b^2 - m_{H^\pm}^2 - \hat{t})D_{22} \\
& +(2m_b^2 - \hat{t} - \hat{u})D_{23})], \\
f_{10} = & -\frac{\alpha_s g m_b}{\sqrt{2}\pi} [h_t m_t \cos \beta (D_0 + 2D_1 + 2D_2 + D_{11} + 2D_{12} + D_{22}) \\
& + \sin \beta h_b m_b (D_1 + D_2 + D_{11} + 2D_{12} + D_{22})], \\
f_{12} = & -\frac{\alpha_s g}{\sqrt{2}\pi} [h_t m_t \cos \beta (D_1 + D_2 + D_{11} + 2D_{12} + D_{13} + D_{22} + D_{23}) \\
& h_b m_b \sin \beta (D_2 + D_{11} + 2D_{12} + D_{13} + D_{22} + D_{23})]. \tag{26}
\end{aligned}$$

The form factors contributing to $\delta M^{V_1(s)}(A)$ are (the argument of the C functions is $[m_b^2, m_b^2, \hat{s}, m_b^2, \lambda^2, m_b^2]$)

$$f_5 = f_9 = \frac{\alpha_s g h_b \sin \beta}{2\sqrt{2}\pi(\hat{s} - m_{A0}^2)} [-1 + 2B_0(m_b^2, m_b^2, \lambda^2) + 2m_b^2 C_0 + \hat{s} C_1 + 2\hat{s} C_2],$$

$$f_6 = f_{10} = -f_5. \quad (27)$$

The form factors which contribute to $\delta M^{V_1(s)}(H)$ are (the argument of the C functions is $[m_b^2, m_b^2, \hat{s}, m_b^2, \lambda^2, m_b^2]$, the form factors to $\delta M^{V_1(s)}(h)$ can be obtained by substituting $\cos \alpha \sin(\alpha - \beta) \rightarrow -\sin \alpha \cos(\alpha - \beta)$)

$$f_5 = f_6 = f_9 = f_{10} = \frac{\alpha_s g h_b \cos \alpha \sin(\alpha - \beta)}{2\sqrt{2}\pi(\hat{s} - m_H^2)} [1 - 2B_0(m_b^2, m_b^2, \lambda^2) - 4m_b^2 C_0 - (2m_b^2 + \hat{s})C_1 - 2\hat{s}C_2]. \quad (28)$$

The form factors which contribute to $\delta M^{V_2(t)}$ are (the argument of the C functions is $[\hat{t}, m_b^2, m_{H^\pm}^2, m_t^2, \lambda^2, m_b^2]$)

$$\begin{aligned} f_1 &= \frac{\alpha_s g m_b}{2\sqrt{2}\pi(\hat{t} - m_t^2)} [h_t m_b m_t \cos \beta (C_0 + C_1) + h_b \sin \beta (-1 + 2B_0(m_b^2, m_b^2, \lambda^2) \\ &\quad + 3m_t^2 C_0 + (-m_b^2 + m_{H^\pm}^2 + m_t^2 + \hat{t})C_1 + (-m_b^2 + 2m_{H^\pm}^2 + m_t^2)C_2)], \\ f_2 &= \frac{\alpha_s g}{2\sqrt{2}\pi(\hat{t} - m_t^2)} [h_t m_t \cos \beta (1 - 2B_0(m_b^2, m_b^2, \lambda^2) - (2m_t^2 + \hat{t})C_0 \\ &\quad + (m_b^2 - m_{H^\pm}^2 - 2\hat{t})C_1 + (m_b^2 - 2m_{H^\pm}^2 - \hat{t})C_2) + h_b m_b \sin \beta (-m_t^2 C_0 \\ &\quad - \hat{t}C_1 + (m_t^2 - \hat{t})C_2)], \\ f_9 &= 2f_3 = 2f_1/m_b. \end{aligned} \quad (29)$$

The scalar integrates B, C, D in above expressions are evaluated by FF package [16].

-
- [1] J.F. Gunion, H.E. Haber, F.E. Paige, W.-K. Tung and S.S.D. Willenbrock, Nucl. Phys. **B294** 621 (1987); C.S. Huang and S.H. Zhu, Phys. Rev. D **60**, 075012 (1999); L. G. Jin, C. S. Li, R. J. Oakes and S. H. Zhu, Phys. Rev. D **62**, 053008 (2000) [arXiv:hep-ph/0003159]; *ibid*, Eur. Phys. J. C **14**, 91 (2000) [arXiv:hep-ph/9907482].
- [2] S. Morreti and K. Odagiri, Phys. Rev. **D55** 5627 (1997).
- [3] E. Eichten, I. Hinchliffe, K. Lane and C. Quigg, Rev. Mod. Phys. **56** (1984) 579. A. Krause, T. Plehn, M. Spira and P. M. Zerwas, Nucl. Phys. **B519** (1998) 85; A. A. Barrientos Bendezu and B. A. Kniehl, Nucl. Phys. **B568** (2000) 305; O. Brein and W. Hollik, Eur. Phys. J. **C13** (2000) 175.
- [4] D.A. Dicus, J.L.Hewett, C. Kao, and T.G. Rizzo, Phys. Rev. **D40**, 789 (1989); A.A. Barrientos Bendezu and B.A. Kniehl, Phys. Rev. **D59**, 015009 (1999); *ibid*, **D63**, 015009 (2001); O. Brein, W. Hollik and S. Kanemura, Phys. Rev. **D63**, 095001 (2001).
- [5] S. Moretti and K. Odagiri, Phys. Rev. **D59**, 055008(1999); K. Odagiri, hep-ph/9901432; Phys. Lett. **B452**, 327(1999); D.P. Roy, Phys. Lett. **B459**, 607 (1999); S. Raychaudhuri and D.P. Roy, Phys. Rev. **D53**, 4902 (1996); M. Beneke, *et al*, hep-ph/0003033, in “Proceedings of the Workshop on Standard Model Physics (and More) at the LHC”, CERN 2000-004, eds. G. Altarelli and M. Mangano.
- [6] Y.S. Yang, C.S. Li, L.G. Jin and S.H. Zhu, Phys.Rev. D **62** (2000) 095012.
- [7] J. Küblbeck, M. Böhm and A. Denner, Comput. Phys. Commun. **60** (1990) 165; T. Hahn, hep-ph/9905354.
- [8] M. Mertig, M. Bohm and A. Denner, Comput. Phys. Commun. **64**, 345 (1991).
- [9] S. Kawabata, Comput. Phys. Commun. **88**, 309 (1995).

- [10] For example to see, S.H. Zhu, hep-ph/0109269, to appear in Phys. Lett. B; T. M. Tait, Phys. Rev. D **61**, 034001 (2000) [hep-ph/9909352].
- [11] See for examples, D.A. Dicus, T. Stelzer, Z. Sullivan and S. Willenbrock, Phys. Rev. D **59**, 094016 (2000) and references therein.
- [12] J. Vermaseren, S. Larin and T. Ritbergen, Phys. Lett. **B405** , 327 (1997).
- [13] Particle Data Group, Eur. Phys.J. C **3**, 1 (1998).
- [14] H.L. Lai, *et al.*(CTEQ collaboration), Eur. Phys.J. C **12** (2000) 375.
- [15] A. Dabelstein, Ph.D. thesis, Munich, 1993, MPI-Ph/93-64; A. Dabelstein, Z. Phys **C 67**, 495 (1995); M. Spira, Fortsch. Phys. **46** (1998) 203.
- [16] G. J. van Oldenborgh and J. A. Vermaseren, Z. Phys. C **46**, 425 (1990).

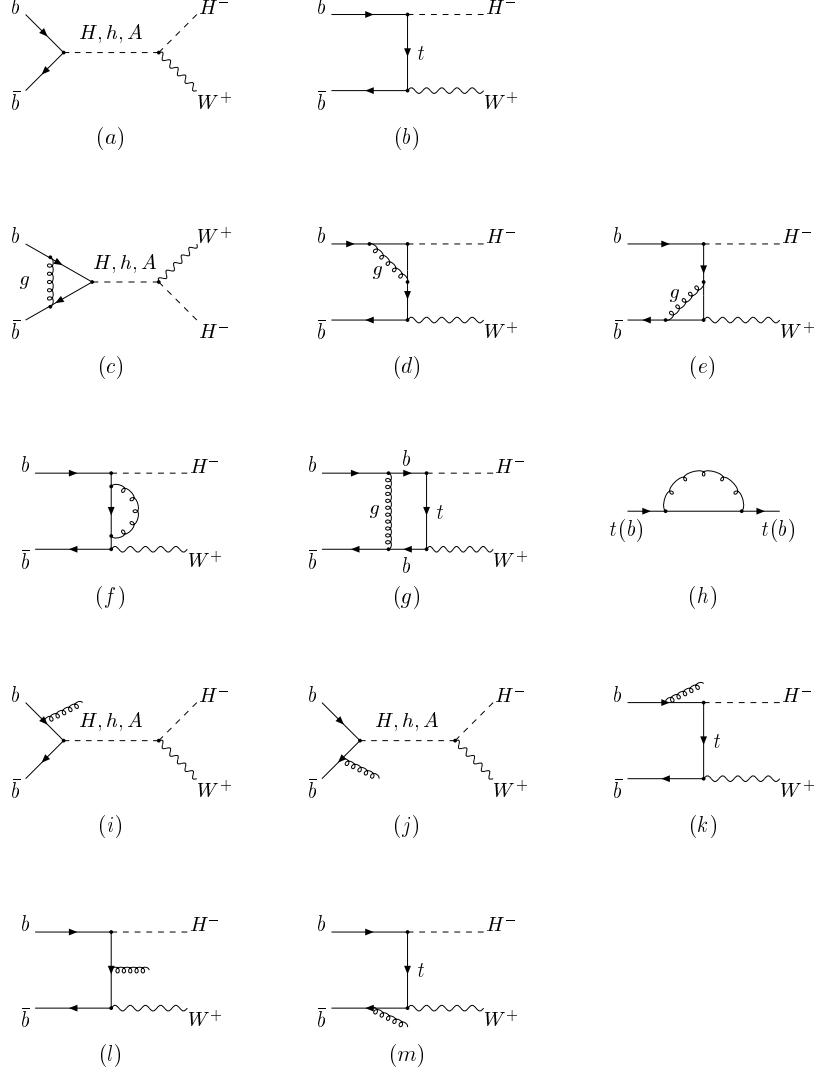


FIG. 1. Feynmann diagrams for the subprocess $b\bar{b} \rightarrow H^- W^+$ at the NLO: (a)-(b) Born diagrams; (c)-(h) virtual correction diagrams; (i)-(m) gluon-radiation diagrams.

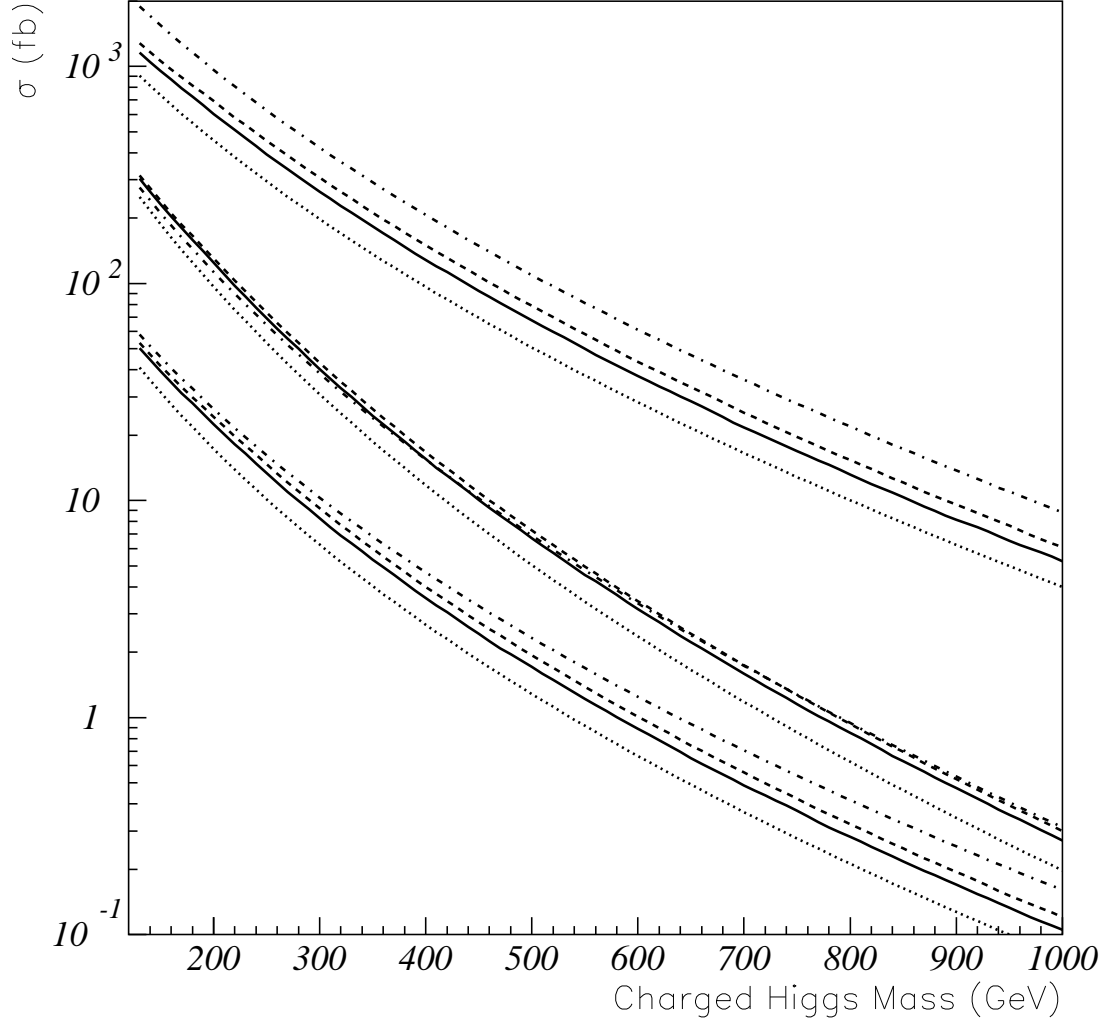


FIG. 2. The total cross sections of process $PP \rightarrow b\bar{b} \rightarrow H^\pm W^\mp$ versus m_{H^\pm} at the LHC with $\sqrt{s} = 14$ TeV in \overline{MS} and OS schemes. The lines correspond to the cross sections at the one-loop level of \overline{MS} (solid), one-loop level of OS (dashed), tree level of \overline{MS} (dotted) and tree level of OS (dash-dotted). The three groups correspond to $\tan \beta = 50, 2, 6$ from above to the bottom.

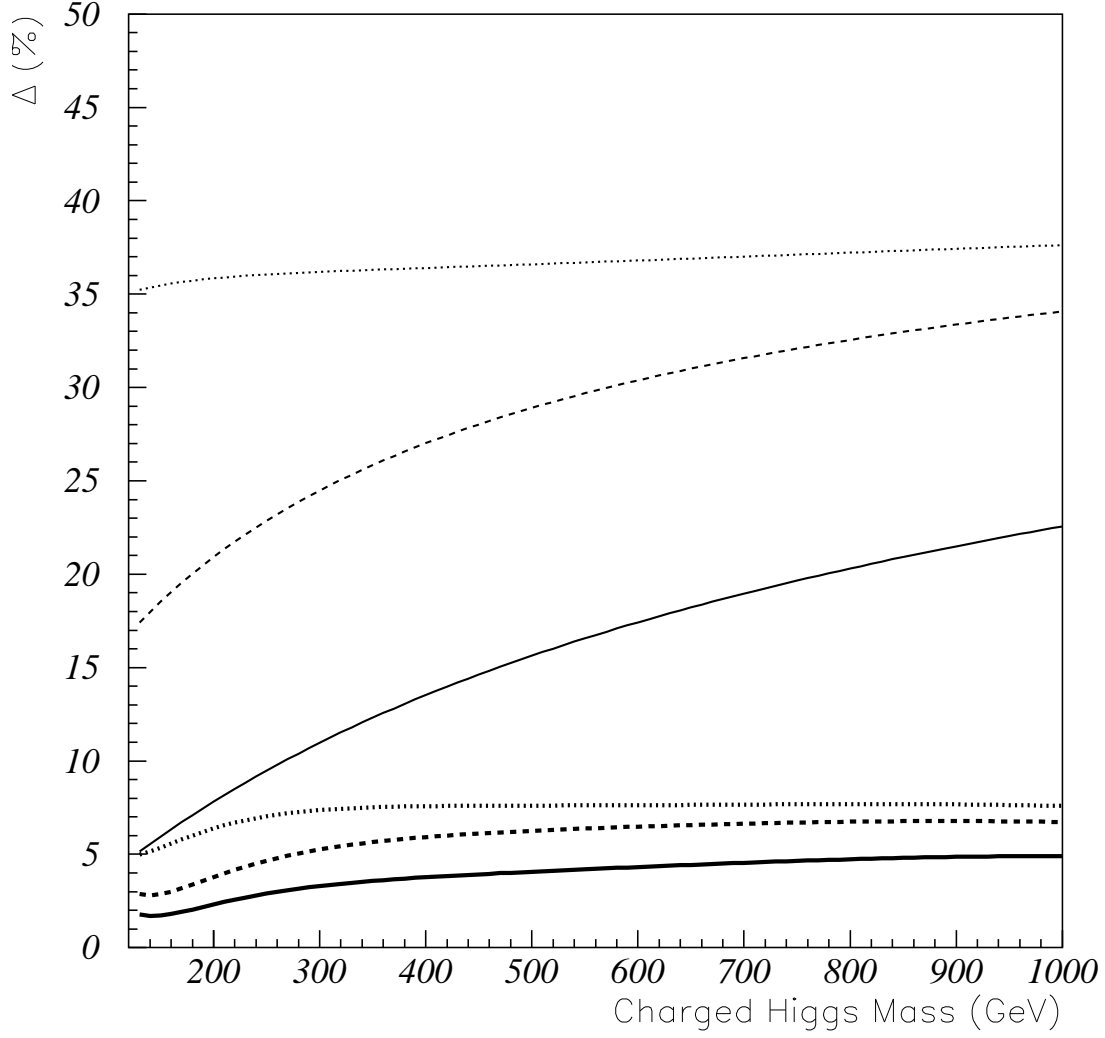


FIG. 3. The Δ (defined in text) versus m_{H^\pm} . The thick lines stand for the results of one-loop and thin lines stand for the results of tree level. $\tan \beta = 2$ (solid), 6 (dashed), 50 (dotted).

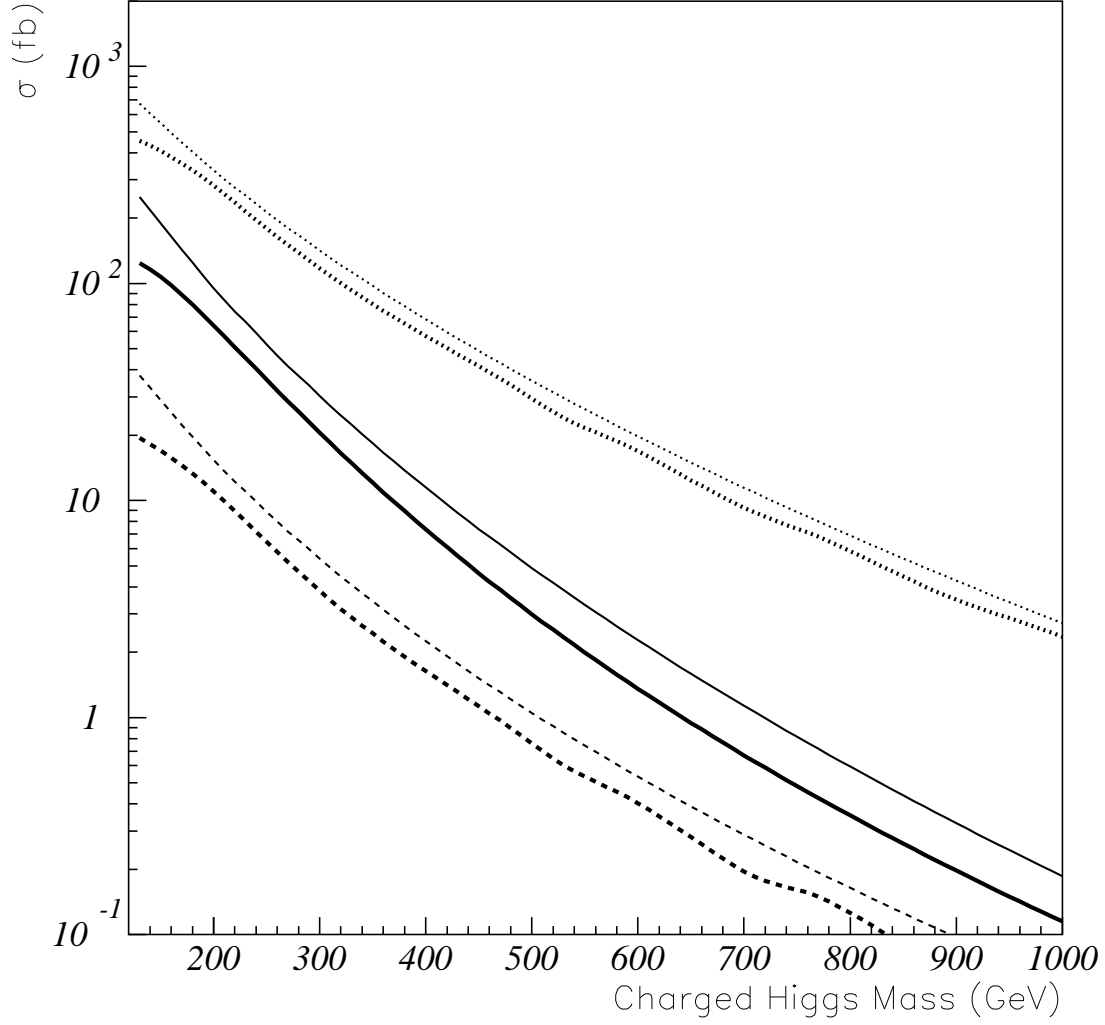


FIG. 4. The total cross sections for the subprocesses $b\bar{b} \rightarrow H^\pm W^\mp$ and $gb(\bar{b}) \rightarrow H^\pm W^\mp b(\bar{b})$ versus m_{H^\pm} at the LHC with $\sqrt{s} = 14$ TeV. The thick lines correspond to the one-loop cross sections with $\tan\beta = 2$ (solid), 6 (dashed) and 50 (dotted). The tree level cross sections are also shown by the corresponding thin lines.

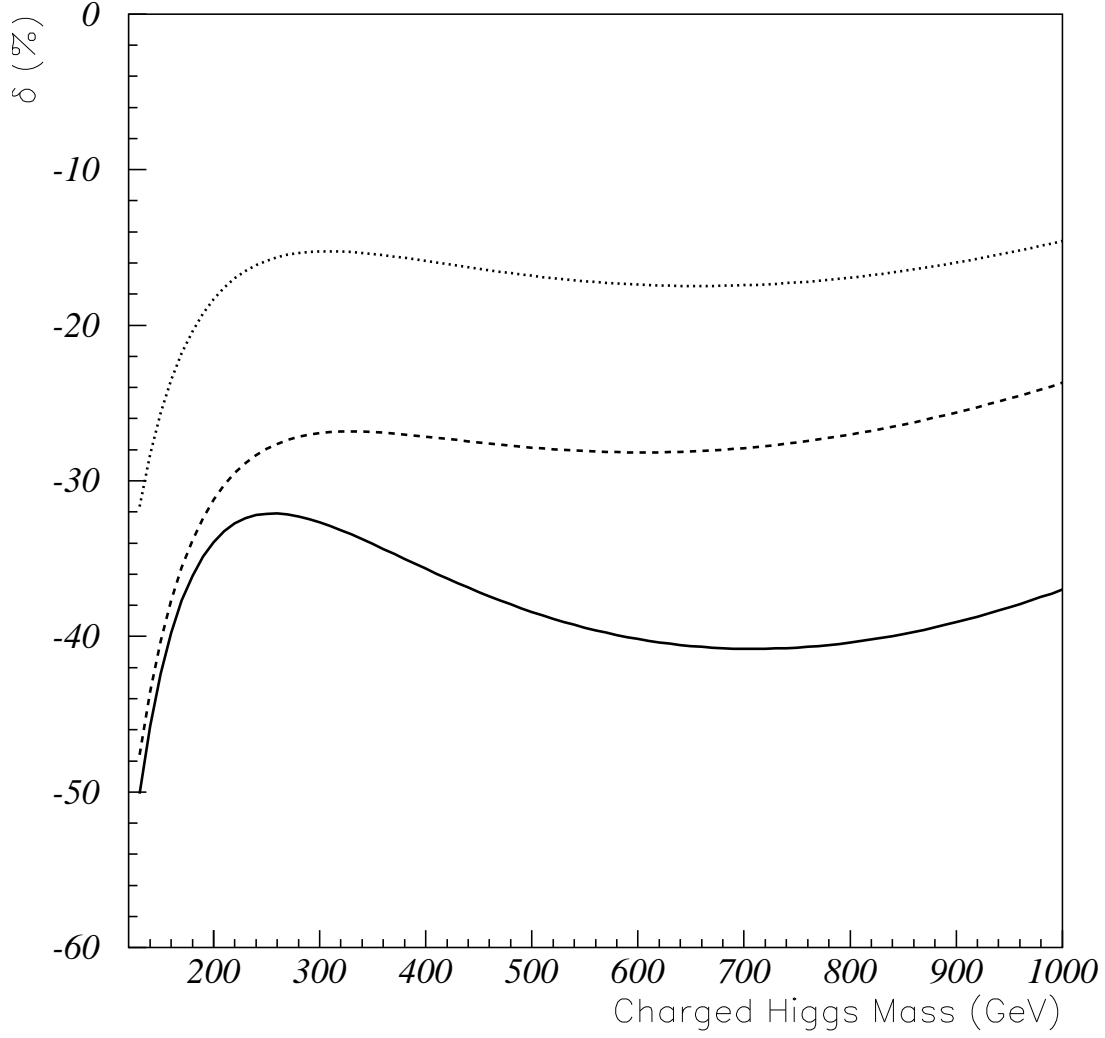


FIG. 5. The QCD relative corrections to the cross sections for the subprocesses $b\bar{b} \rightarrow H^\pm W^\mp$ and $gb(\bar{b}) \rightarrow H^\pm W^\mp b(\bar{b})$ versus m_{H^\pm} . The lines correspond to $\tan\beta = 2$ (solid), 6(dashed) and 50(dotted).

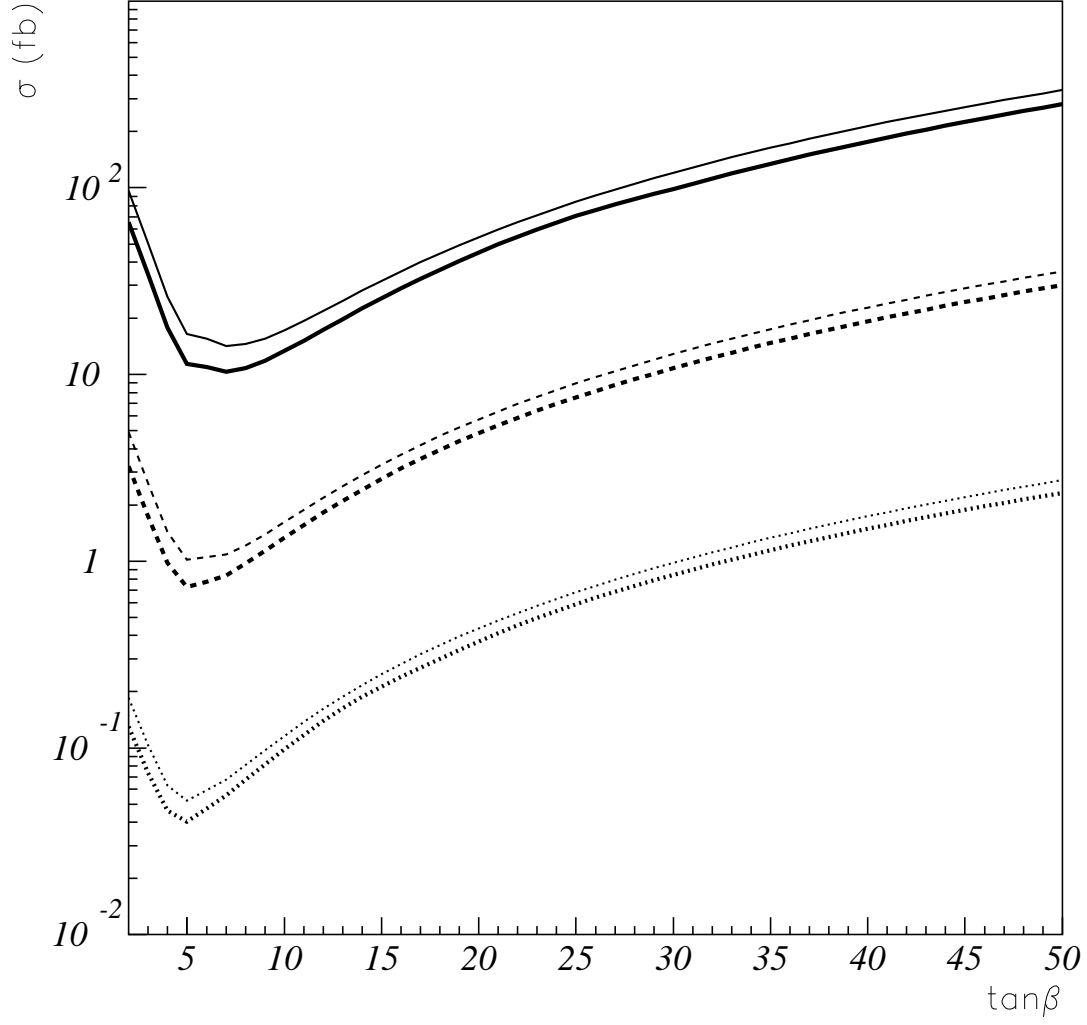


FIG. 6. Same as Fig. 4 except versus $\tan\beta$. The lines correspond to $m_{H^\pm} = 200$ (solid), 500(dashed) and 1000 GeV (dotted).

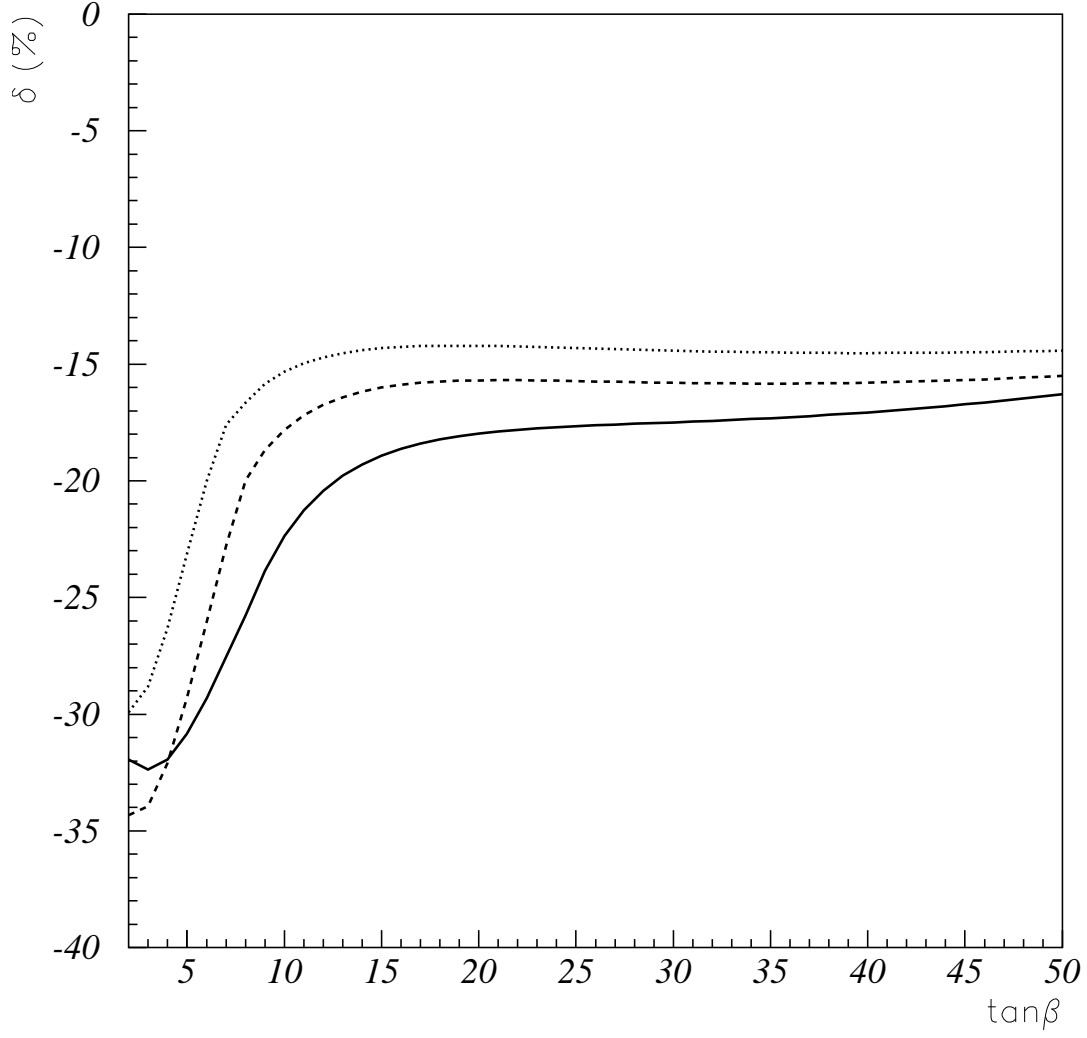


FIG. 7. Same as Fig. 5 except versus $\tan \beta$. The lines correspond to $m_{H^\pm} = 200$ (solid), 500(dashed) and 1000 GeV (dotted).

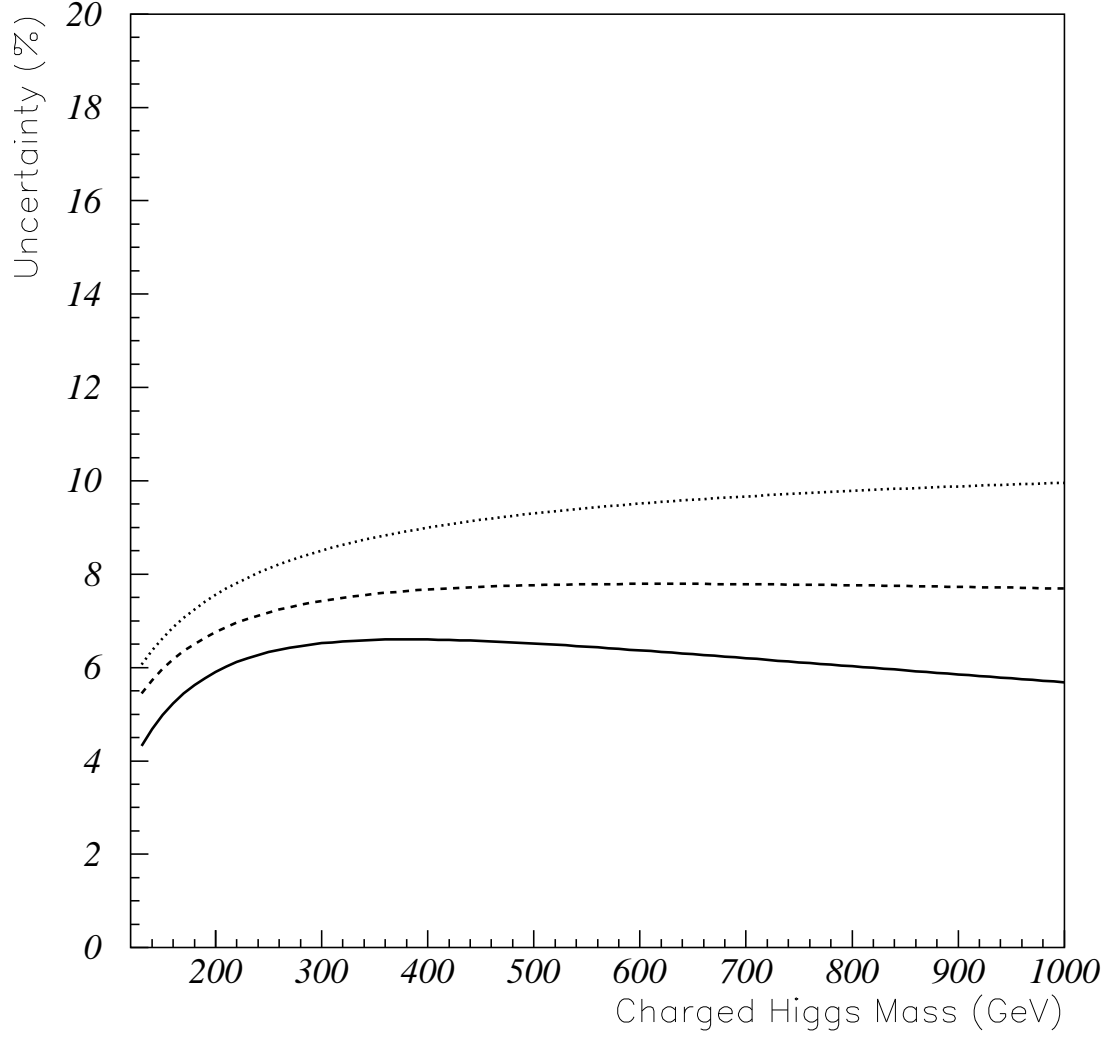


FIG. 8. The uncertainty [defined in Eq. (23)] as a function of m_{H^\pm} , where the renormalization scale is fixed as $m_{H^\pm} + m_W$. The lines correspond to $\tan \beta = 2$ (solid), 6(dashed) and 50(dotted).

m_{H^\pm} (GeV)	$\tan \beta = 50$	$\tan \beta = 2$
200	$\sim -16\%$	$\sim -32\%$
500	$\sim -15\%$	$\sim -34\%$
1000	$\sim -14\%$	$\sim -30\%$

TABLE I. QCD corrections to the process $b\bar{b} \rightarrow H^\pm W^\mp$ in MSSM and 2HDM in \overline{MS} scheme.

The renormalization and factorization scales are taken as $m_{H^\pm} + m_W$.